Determination of the element-specific complex permittivity using a soft x-ray phase modulator

Y. Kubota,[1] Y. Hirata,[1] J. Miyawaki,[1] S. Yamamoto,[1] H. Akai,[1] R. Hobara,[2] Sh. Yamamoto,[1] K. Yamamoto,[1] T. Someya,[1] K. Takubo,[1] Y. Yokoyama,[1] M. Araki,[1] M. Taguchi,[3] Y. Harada,[1] H. Wadati,[1] M. Tsunoda,[4] R. Kinjo,[5] A. Kagamihata,[5] T. Seike,[5] M. Takeuchi,[5] T. Tanaka,[5] S. Shin,[1] and I. Matsuda[1,*]

[1]*Institute for Solid State Physics, The University of Tokyo, Kashiwa, Chiba 277-8581, Japan*

[2]*Department of Physics, The University of Tokyo, Bunkyo-ku, Tokyo 113-0033, Japan*

[3]*Nara Institute of Science and Technology (NAIST), Ikoma, Nara 630-0192, Japan*

[4]*Department of Electronic Engineering, Tohoku University, Sendai, Miyagi 980-8579, Japan*

[5]*RIKEN SPring-8 Center, Sayo, Hyogo 679-5148, Japan*

(Received 20 May 2017; revised manuscript received 15 November 2017; published 11 December 2017)

We report on directly determining the complex permittivity tensor using a method combining a developed light source from a segmented cross undulator of synchrotron radiation and the magneto-optical Kerr effect. The empirical permittivity, which carries the electronic and magnetic information of a material, has element specificity and has perfect confirmation using the quantum-mechanical calculation for itinerant electrons systems. These results help in understanding the interaction of light and matter, and they provide an interesting approach to seek the best materials as optical elements, for example, in extended-ultraviolet lithographic technologies or in state-of-the-art laser technologies.

DOI: 10.1103/PhysRevB.96.214417

I. INTRODUCTION

Permittivity (or conductivity) is a quantity that characterizes the material response to an electric field, such as electromagnetic waves [1–3]. Historically, such responses have been exploited to develop a variety of electronic and optical devices that have supported our society today. The determination and understanding of the permittivity of materials has been one of the highest priority tasks in science and technology [4–12]. Recently, material specifications have entered the extended-ultraviolet (EUV)–soft x-ray (SX) region because of the need to develop, for example, EUV lithography applied in advanced technology developments or ultrahigh-resolution SX experimental research at the frontier of science [13,14]. Determination of the complex optical constants by resonant SX scattering has also become critical in evaluating structural and electronic properties of organic films [15,16].

Permittivity has often been approximated as a (dielectric) constant but is in essence a tensor quantity with diagonal and off-diagonal components [1–3]. The two types of components carry the nonmagnetic and the magnetic information regarding the response of the material, and it is the latter that has been significant in understanding spin polarization or magnetization. The individual components are complex, being composed of a real and an imaginary part. Their determination has been widely made using a probe light with a polarization modulation (frequency of p) and the measurement of the optical responses of the sample at the two frequencies $(p, 2p)$ [4,17]. Such an experiment is easily performed by transmitting the incident light through crystals that allow electric or mechanic controls of the polarization. Indeed, one can find a variety of commercial polarization modulators for visible light and hard x rays [17,18] but not for the EUV-SX region. This is mainly because the absorbance of light in matter in this region is so large that transmission is not possible; light only survives in a vacuum in the absence of air molecules. In addition, the "abnormal" optical response at the absorption edges for the elements in the composition also intervenes in the precise evaluation. To date, the determination has been made with the help of simulations with models based on atomic parameters and indirect experimental data, often with large errors being propagated via the uncertainties associated with permittivities. To overcome these difficulties, one can use synchrotron radiation (SR), generated by electrons, that already exists in the vacuum and one can control the polarization using the electron trajectory which can be regulated by an external magnetic field [19–21].

In this paper, we developed a SX source for a segmented cross undulator enabling the polarization modulation (p) of light to be performed continuously and magneto-optical measurements $(p, 2p)$ of a buried Fe nanofilm to be carried out at the Fe L-shell absorption edge in the SX region. Although the magneto-optical effects of magnetic materials in this energy region have been investigated for many years [22–30], we have succeeded in directly determining the complex components of the permittivity tensor and we found that the first-principles calculation within the Korringa-Kohn-Rostoker (KKR) formalism gave perfect matching results. Our procedure determines the permittivity of a sample in the EUV-SX region with high precision, which is important for a better understanding of the interaction of light and matter. It also provides a different technical method of examination to seek the best materials as optical elements, for example, in EUV lithographic technologies or in laser technologies using high-harmonic generation lasers, high-brilliant SR, and the x-ray free electron laser (XFEL)[13,14,31,32].

II. EXPERIMENT

Continuous polarization modulation of a SX source was achieved from the segmented cross undulator, developed at SPring-8 BL07LSU [33]. It is composed of two types of undulators and phase shifters. The former generates semicoherent

*imatsuda@issp.u-tokyo.ac.jp

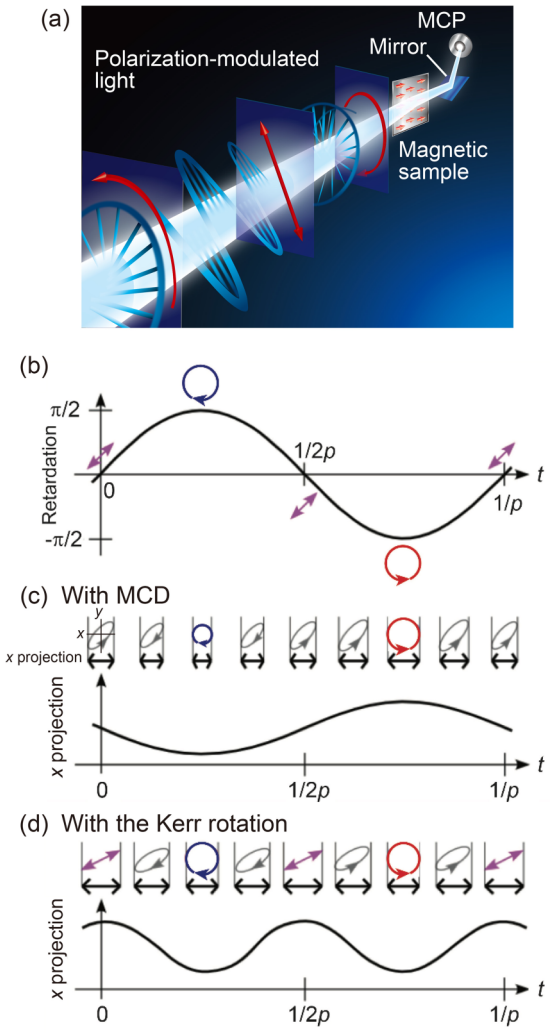

FIG. 1. (a) Image of the polarization-modulated light with the L-MOKE setup. (b) Time dependence of the retardation $\delta = (\pi/2)\sin 2\pi pt$. The polarization of light with retardation δ varies skew linearly (SL) → right-handed circular→ SL → left-handed circular→ SL. (c) and (d) Schematic for why the p and $2p$ components represent MCD and the Kerr rotation, respectively. Projections onto the x axis of the electric field reflected from samples (c) with MCD and (d) with the Kerr rotation [17].

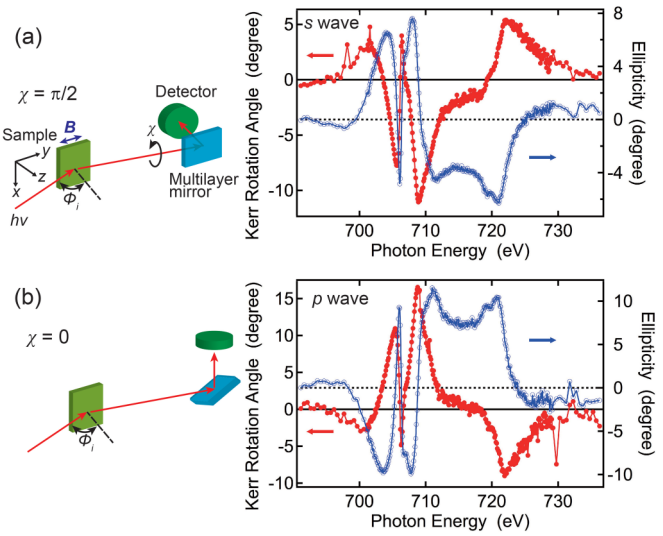

FIG. 2. Geometries and results of L-MOKE measurements for an Fe nanofilm at the L-edge using the polarization-modulated light for (a) the s wave and (b) the p wave. Red solid circles and blue open circles represent the spectra of θ_K (left axis) and ε_K (right axis), respectively.

light with either horizontal or vertical linear polarization. The latter controls the phase retardation of the electromagnetic waves from the undulators resulting in various polarized SX beams being produced at the experimental station. A continuous phase shift is obtained magnetically using an electromagnetic coil to introduce an additional path for the relativistic electron [34]. The polarization modulation (see Fig. 1) is achieved using a sinusoidal alternating current (ac). As for a piezo-birefringent modulator for visible light, the periodically varying retardation is given as

$$\delta = \delta_0 \sin 2\pi pt, \tag{1}$$

where δ_0 and p represent the retardation amplitude and modulation frequency, respectively. Setting $\delta_0 = \pi/2$, the light polarization can be varied continuously from linear to right- or left-handed circular. When using this polarization-modulated beam in magneto-optical experiments, the ellipticity (ε_K) appears in signals as the p component by the magnetic circular dichroism (MCD), whereas the $2p$ component depends on the Kerr rotation angle (θ_K) by the optical rotation. That is, by extracting the p and $2p$ components, ε_K and θ_K are measurable simultaneously. Moreover, the signals are detected with high sensitivity because the measurement system intrinsically contains lock-in amplification.

The measurement system to detect the magneto-optical effect consists of a polarizer and an optical analyzer to detect a change in the light polarization after reflection by a magnetic sample. The role of the polarizer is achieved by adoption of the polarization-controlled SX source. The analyzer in the SX region is composed of a (multilayer) mirror and a photon detector (microchannel plate, MCP). The polarization analysis is made by the rotating analyzer ellipsometry (RAE), which measures light intensity as a function of angle (χ) around an axis between the mirror and the sample. We set $\chi = \pi/2$ when the multilayer mirror reflects the light in the z direction [Fig. 2(a)]. Then, with the longitudinal MOKE (L-MOKE) configuration, θ_K and ε_K for the s-polarized incident light, distinguished by a superscript s, can be written in terms of the intensities [$I(0)$, $I(p)$, and $I(2p)$] at the frequency-independent offset, p, and $2p$ components as follows:

$$\begin{aligned} I(0) &= C_s\left\{1 + \theta_K^{s2} + \varepsilon_K^{s2} + 2\theta_K^s J_0(\delta_0)\right\}, \\ I(p) &= 4C_s\varepsilon_K^s J_1(\delta_0), \\ I(2p) &= 4C_s\theta_K^s J_2(\delta_0), \end{aligned} \tag{2}$$

where C_s is a constant of proportionality and $J_n(\delta_0)$ is the nth order Bessel function. In contrast, when the multilayer mirror reflects the light in the x direction [Fig. 2(b)], for which $\chi = 0$, θ_K and ε_K for the p-polarized incident light, distinguished by

a superscript p, is obtained from the intensities:

$$I(0) = C_p\{1 + \theta_K^{p2} + \varepsilon_K^{p2} + 2\theta_K^p J_0(\delta_0)\},$$
$$I(p) = -4C_p\varepsilon_K^p J_1(\delta_0),$$
$$I(2p) = 4C_p\theta_K^p J_2(\delta_0). \quad (3)$$

Here C_p is the constant of proportionality for the p wave. More details about Eqs. (2) and (3) are described in the Appendix.

In this study, a Ta/Cu/Fe/MgO heterostructure sample was used in the L-MOKE experiment. By magnetron sputtering, a 30-nm-thick Fe nanofilm was epitaxially grown on the MgO(001) substrate and then capped with Ta (2 nm thick) and Cu (2 nm thick) layers to prevent the Fe layer from oxidizing. The Fe nanofilm has an in-plane easy direction of magnetization. The angle of incidence ϕ_i of the modulated SR beam onto the sample was about 80° with respect to the surface normal in the yz plane [Fig. 2(a)]. Using a split-coil magnet, a magnetic field B of strength ±0.3 T, under which the magnetization of the Fe nanofilm was saturated, was applied along the y direction. The sample was maintained at room temperature during measurements.

The off-diagonal components of permittivity for bulk Fe (bcc) were calculated by the KKR-Green's function method using Machikaneyama (AkaiKKR), a KKR-CPA-LDA package [35]. In this first-principles calculation, the electronic structure is calculated within the framework of the local-density approximation (LDA) of the density functional theory. The relativistic effects are included for both the core and the valence states. Further details of the method can be found in the article by Akai [36].

III. RESULTS AND DISCUSSION

Figure 2 shows the results for the simultaneous measurement of θ_K and ε_K for the Fe nanofilm taken at $\chi = \pi/2$ (s-wave configuration) and $\chi = 0$ (p wave) using the L-MOKE configuration. The absolute values were calibrated by degrees of light polarization. The phase of the light polarization in Eq. (1) was modulated with the following settings: ac 25 ± 0.588 A and frequency $p = 12.987$ Hz. The ac modulation of 0.588 A corresponds to $\delta_0 = \pi/2$.

Fine spectral features can be seen in the two signals. Moreover, the θ_K and ε_K spectra appear to be derivatives of each other, which is consistent with the relationship expressed by the Kramers-Kronig relations [3,24]. It is notable that these ε_K spectra were first directly observed in the SX region.

Based on the electromagnetic theory, $(\theta_K^s, \varepsilon_K^s)$ and $(\theta_K^p, \varepsilon_K^p)$ in the L-MOKE geometry are expressed as [3]

$$\theta_K^s + i\varepsilon_K^s = -r_{ps}/r_{ss} \approx \frac{-in_0nQ}{(n^2 - n_0^2)}\frac{\cos\phi_i \tan\phi_t}{\cos(\phi_i - \phi_t)}, \quad (4)$$

$$\theta_K^p + i\varepsilon_K^p = -r_{sp}/r_{pp} \approx \frac{-in_0nQ}{(n^2 - n_0^2)}\frac{\cos\phi_i \tan\phi_t}{\cos(\phi_i + \phi_t)}, \quad (5)$$

where the complex Fresnel coefficient, r_{ij}, denotes the ratio of the incident j-polarized electric field and the reflected i-polarized electric field; n and n_0 represent the complex constants of refraction for the Fe nanofilm and the capping layer (Ta/Cu), respectively. When ϕ_i is large ($70° \leqslant \phi_i \leqslant 90°$) and $\phi_i \approx \phi_t$, the sign changes between θ_K^s and θ_K^p and between ε_K^s and ε_K^p, because of the cosine function in the denominator [27,37,38]. The behavior is consistent with the spectra given in Fig. 2.

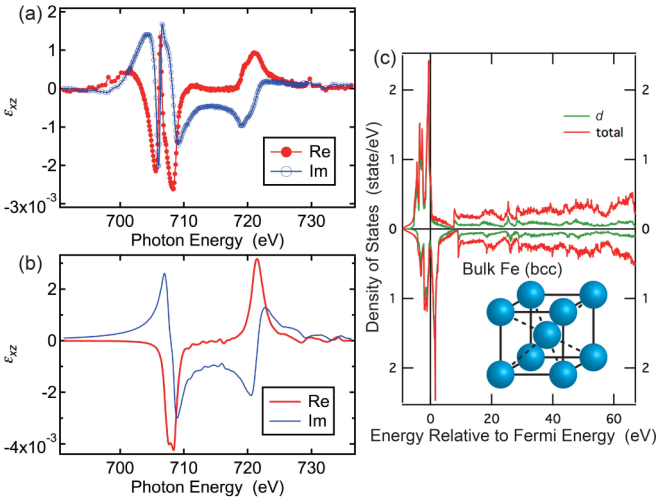

FIG. 3. (a) ϵ_{xz} spectra of the Fe nanofilm at the L edge obtained from L-MOKE measurements with polarization-modulated light. Red solid circles and blue open circles represent its real and imaginary parts, respectively. (b) ϵ_{xz} spectra of bulk Fe (bcc) at the L edge obtained using the first-principles calculation within the KKR formalism. Red and blue lines represent its real and imaginary parts, respectively. (c) Density of states of bulk Fe (bcc) calculated using the first-principles calculation. Red and green lines represent the density of states of all states and the d state, respectively. The inset illustrates the crystal structure of bulk Fe (bcc).

The magneto-optical quantities are governed by the Voigt parameter Q, as is apparent in Eqs. (4) and (5), which depends on a specific ratio of two components of the permittivity tensor,

$$Q = i\frac{\epsilon_{xz}}{\epsilon_{xx}}, \quad (6)$$

where the permittivity tensor takes the form

$$\epsilon = \begin{pmatrix} \epsilon_{xx} & 0 & \epsilon_{xz} \\ 0 & \epsilon_{yy} & 0 \\ -\epsilon_{xz} & 0 & \epsilon_{zz} \end{pmatrix}. \quad (7)$$

The diagonal component, ϵ_{xx}, is given as $\epsilon_{xx} = n^2$ and carries non-magneto-optical information of a sample, whereas ϵ_{xz} contains the magneto-optical properties. Hence, with the given values of n and n_0 as well as the measurement conditions of ϕ_i and ϕ_t, ϵ_{xz} can be evaluated from Eqs. (4)–(6) [25,39].

Figure 3(a) shows the ϵ_{xz} spectra of the Fe nanofilm. One finds again that the Kramers-Kronig relations hold for the real and the imaginary parts. We also studied the permittivity of bulk Fe (bcc) by performing the first-principles calculation within the KKR formalism; the calculated spectra are shown in Fig. 3(b). One finds good agreement between the experimental and theoretical ϵ_{xz} spectra. For the first time, these results indicate that the present method and the theoretical approach are reliable in determining the off-diagonal component in the SX region. On the other hand, compared to the simulation,

one can find additional structures, the dip in the Im curve and the peak in Re curve at the L_3 edge, in the experimental spectra. These features originate from the magneto-optical spectra in Fig. 2 that appear to stem from the interference effects, as discussed in previous L-edge MOKE studies [26,27,38]. The apparent reproduction from the first-principles calculation indicates that the method is useful in evaluating the spin-polarized electronic structure of materials. Moreover, detailed analysis on the interference effect would also reveal structural and electronic properties of a nanofilm and the interfaces.

IV. SUMMARY

In summary, we have described the development of a SX magneto-optical spectroscope that uses a SX source from the segmented cross undulator. This method offers various advantages for material science and technology. A complete data set of real and imaginary parts of the complex ϵ_{xz} can be determined simultaneously with high sensitivity through the lock-in amplification inherently adopted in the measurement system. Thus, faint magnetic signals are able to be detected; moreover, the data sets are self-consistent with the Kramers-Kronig relations. This provides benefits when investigating new magnetic materials as well as for evaluating nonuniform systems, such as nanopatterned structures or heterostructures. By tuning the probe photon energy at the absorption edge, as performed in the present study, the data have element selectivity, which is suitable for studying multielement samples. Extension to different photon energies, such as in the EUV region or at other absorption edges of elements in different materials, is easily achieved by changing the electron energy and the magnetic field in an undulator and also by replacing a (multilayer) mirror in the optical analyzer. As the permittivity is essential for optical elements, the present evaluation procedure is significant in that it advances both EUV lithography technology and high-resolution SX spectroscopy [13,14].

Note that the present research parallels that on the inverse Faraday effect [31,32], which has currently attracted great interest in the field of ultrafast spintronics. Using an optical pulse, the effect induces spin-flipping that depends on permittivity. Thus, spin regulation can be element specific if one uses an XFEL at the absorption edge. The present method may open a similar field of research on extreme optical science of condensed matter.

ACKNOWLEDGMENTS

This research was partially supported by the Ministry of Education, Culture, Sports, Science, and Technology of Japan (X-ray Free Electron Laser Priority Strategy Program and Photon and Quantum Basic Research Coordinated Development Program), the Research Foundation for Opto-Science and Technology, the Hyogo Science and Technology Association, and the Japan Society for the Promotion of Science under a Grant-in-Aid for Scientific Research (C) (Grant No. 26400328). The experiment was performed using the facilities of the Synchrotron Radiation Research Organization, The University of Tokyo (Proposals No. 2014A7401, No. 2014B7401, No. 2014B7473, No. 2015A7401, No. 2015B7401, No. 2016A7403, No. 2016A7504, and No. 2016B7403). We thank Masato Kotsugi for valuable discussion and Hiroshi Narita for building the experimental equipment. Yoshinobu Takahashi is acknowledged for his support during the experiment. M.T. acknowledges Hiroshi Daimon for supporting his research with valuable discussion. Y.K. acknowledges support from the ALPS programs of the University of Tokyo.

APPENDIX: MOKE METHOD COMBINING THE POLARIZATION-MODULATED SX

This Appendix provides detailed additional information about the MOKE method, especially the L-MOKE geometry, combining the RAE and the polarization-modulated SX.

First, the electric field vector of the skew-linear polarized light with 45° tilt is expressed as

$$\boldsymbol{E}_{\rm in} = \frac{E_0}{\sqrt{2}}(\boldsymbol{i} + \boldsymbol{j}), \tag{A1}$$

where $\boldsymbol{i}$ and $\boldsymbol{j}$ represent unit vectors along the p- and s-wave directions, respectively. E_0 is the amplitude of the electric field for both of the p and s components. After addition of the retardation $\delta = \delta_0 \sin 2\pi pt$, $\boldsymbol{E}_{\rm in}$ is rewritten as

$$\boldsymbol{E}_{\rm in} = \frac{E_0}{\sqrt{2}}(\boldsymbol{i} + e^{i\delta}\boldsymbol{j}). \tag{A2}$$

When this modulated light is incident onto a magnetic sample, the electric field vector of the reflected light $\boldsymbol{E}_{\rm out}$ is described by using the complex Fresnel coefficients:

$$\boldsymbol{E}_{\rm out} = \frac{E_0}{\sqrt{2}}\{(r_{pp} - e^{i\delta}r_{sp})\boldsymbol{i} + (-r_{sp} + e^{i\delta}r_{ss})\boldsymbol{j}\}. \tag{A3}$$

Here, we change the unit vectors to those along the p- and s-wave directions for the multilayer mirror in the RAE unit, $\boldsymbol{p}_{\rm A}$ and $\boldsymbol{s}_{\rm A}$. $\boldsymbol{E}_{\rm out}$ can be rewritten as

$$\begin{aligned}\boldsymbol{E}_{\rm out} = \frac{E_0}{\sqrt{2}}[&\{\cos\chi(r_{pp} - e^{i\delta}r_{sp}) + \sin\chi(-r_{sp} \\ &+ e^{i\delta}r_{ss})\}\boldsymbol{s}_{\rm A} + \{-\sin\chi(r_{pp} - e^{i\delta}r_{sp}) \\ &+ \cos\chi(-r_{sp} + e^{i\delta}r_{ss})\}\boldsymbol{p}_{\rm A}],\end{aligned} \tag{A4}$$

where the rotation angle of the RAE unit, χ, is defined as an angle between the $\boldsymbol{j}$ direction and the $\boldsymbol{p}_{\rm A}$ direction (or the $\boldsymbol{i}$ direction and the $\boldsymbol{s}_{\rm A}$ direction), as shown in Fig. 4. The intensity I detected by the detector in the RAE unit is expressed as

$$\begin{aligned}I = |\boldsymbol{E}_{\rm out}|^2 = \frac{E_0^2}{2}\big\{&R_{s_{\rm A}}^2|\cos\chi(r_{pp} - e^{i\delta}r_{sp}) \\ &+ \sin\chi(-r_{sp} + e^{i\delta}r_{ss})|^2 \\ &+ R_{p_{\rm A}}^2|-\sin\chi(r_{pp} - e^{i\delta}r_{sp}) \\ &+ \cos\chi(-r_{sp} + e^{i\delta}r_{ss})|^2\big\},\end{aligned} \tag{A5}$$

where $R_{s_{\rm A}}$ and $R_{p_{\rm A}}$ represent the reflection rate of the multilayer mirror for the s and p waves, respectively. Because the multilayer mirror can mostly reflect only the s wave, it is reasonable to approximate $R_{s_{\rm A}}/R_{p_{\rm A}} \gg 1$; thus, the intensity I

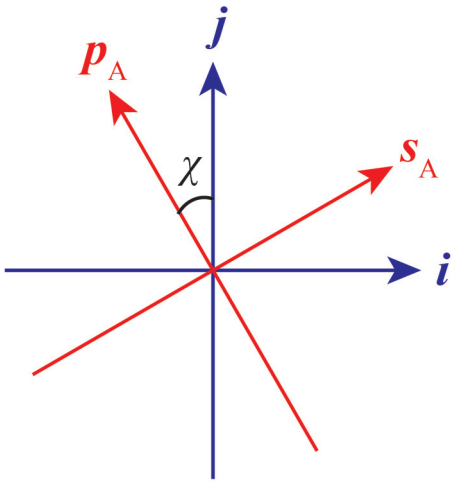

FIG. 4. Relation between the unit vectors $\boldsymbol{i}$, $\boldsymbol{j}$, $\boldsymbol{s}_{\mathrm{A}}$, and $\boldsymbol{p}_{\mathrm{A}}$ and the rotation angle χ.

can be calculated by

$$I \approx \frac{E_0^2}{2} R_{s_{\mathrm{A}}}^2 |\cos\chi(r_{pp} - e^{i\delta} r_{sp}) + \sin\chi(-r_{sp} + e^{i\delta} r_{ss})|^2. \tag{A6}$$

When $\chi = 0$, that is to say, the multilayer mirror reflects the light in the $\boldsymbol{j}$ direction (vertical) [see Fig. 2(b)], I is calculated by using Eq. (5):

$$I \approx \frac{E_0^2}{2} R_{s_{\mathrm{A}}}^2 r_{pp}^2 \left|1 - \frac{r_{sp}}{r_{pp}} e^{i\delta}\right|^2 \tag{A7}$$

$$= C_p \left|1 + \left(\theta_{\mathrm{K}}^p + i\varepsilon_{\mathrm{K}}^p\right) e^{i\delta}\right|^2 \tag{A8}$$

$$= C_p \left\{1 + \theta_{\mathrm{K}}^{p2} + \varepsilon_{\mathrm{K}}^{p2} - 2\varepsilon_{\mathrm{K}}^p \sin(\delta_0 \sin pt) + 2\theta_{\mathrm{K}}^p \cos(\delta_0 \sin pt)\right\}, \tag{A9}$$

where C_p represents a proportional constant. As one can see, when $\chi = 0$, θ_{K} and ε_{K} for the p-polarized incident light, θ_{K}^p and $\varepsilon_{\mathrm{K}}^p$, can be observed. Furthermore, by using the following expansion formulas,

$$\cos(\delta_0 \sin pt) = J_0(\delta_0) + 2J_2(\delta_0)\cos 2pt + \cdots, \tag{A10}$$

$$\sin(\delta_0 \sin pt) = 2J_1(\delta_0)\sin pt + \cdots, \tag{A11}$$

where $J_n(x)$ represents the nth order Bessel function, we can calculate

$$I \approx C_p \left\{1 + \theta_{\mathrm{K}}^{p2} + \varepsilon_{\mathrm{K}}^{p2} + 2\theta_{\mathrm{K}}^p J_0(\delta_0) - 4\varepsilon_{\mathrm{K}}^p J_1(\delta_0)\sin pt + 4\theta_{\mathrm{K}}^p J_2(\delta_0)\cos 2pt + \cdots\right\} \tag{A12}$$

$$\approx I(0) + I(p)\sin pt + I(2p)\cos 2pt, \tag{A13}$$

in which

$$I(0) = C_p \left\{1 + \theta_{\mathrm{K}}^{p2} + \varepsilon_{\mathrm{K}}^{p2} + 2\theta_{\mathrm{K}}^p J_0(\delta_0)\right\},$$
$$I(p) = -4C_p \varepsilon_{\mathrm{K}}^p J_1(\delta_0),$$
$$I(2p) = 4C_p \theta_{\mathrm{K}}^p J_2(\delta_0), \tag{A14}$$

where $I(0)$, $I(p)$, and $I(2p)$ represent the intensity of the frequency-independent offset, p, and $2p$ components, respectively.

On the other hand, when $\chi = \pi/2$, that is to say, the multilayer mirror reflects the light in the $\boldsymbol{i}$ direction (horizontal) [see Fig. 2(a)], Eq. (A6) is calculated as

$$I \approx \frac{E_0^2}{2} R_{s_{\mathrm{A}}}^2 r_{ss}^2 \left|e^{i\delta} - \frac{r_{ps}}{r_{ss}}\right|^2 \tag{A15}$$

$$= C_s \left|e^{i\delta} + \left(\theta_{\mathrm{K}}^s + i\varepsilon_{\mathrm{K}}^s\right)\right|^2 \tag{A16}$$

$$= C_s \left\{1 + \theta_{\mathrm{K}}^{s2} + \varepsilon_{\mathrm{K}}^{s2} + 2\varepsilon_{\mathrm{K}}^s \sin(\delta_0 \sin pt) + 2\theta_{\mathrm{K}}^s \cos(\delta_0 \sin pt)\right\}, \tag{A17}$$

where C_s represents a proportional constant. In contrast to $\chi = 0$, when $\chi = \pi/2$, we can observe θ_{K} and ε_{K} for the s-polarized incident light, θ_{K}^s and $\varepsilon_{\mathrm{K}}^s$. In the same way as $\chi = 0$, we obtain

$$I \approx C_s \left\{1 + \theta_{\mathrm{K}}^{s2} + \varepsilon_{\mathrm{K}}^{s2} + 2\theta_{\mathrm{K}}^s J_0(\delta_0) + 4\varepsilon_{\mathrm{K}}^s J_1(\delta_0)\sin pt + 4\theta_{\mathrm{K}}^s J_2(\delta_0)\cos 2pt + \cdots\right\} \tag{A18}$$

$$\approx I(0) + I(p)\sin pt + I(2p)\cos 2pt, \tag{A19}$$

in which

$$I(0) = C_s \left\{1 + \theta_{\mathrm{K}}^{s2} + \varepsilon_{\mathrm{K}}^{s2} + 2\theta_{\mathrm{K}}^s J_0(\delta_0)\right\},$$
$$I(p) = 4C_s \varepsilon_{\mathrm{K}}^s J_1(\delta_0),$$
$$I(2p) = 4C_s \theta_{\mathrm{K}}^s J_2(\delta_0). \tag{A20}$$

In summary, in contrast to the normal MOKE measurement where linearly fixed polarization is used, χ should be fixed in the MOKE measurement with the polarization-modulated SX. It contributes to reduction of the measurement time. Moreover, the MOKE measurements for the s- and p-polarized incident lights can be switched by changing χ.

[1] L. L. Landau and E. M. Lifshitz, *Electrodynamics of Continuous Media* (Pergamon, Elmsford, NY, 1960).
[2] B. Donovan and T. Medcalf, Proc. Phys. Soc. **86**, 1179 (1965).
[3] P. M. Oppeneer, in *Handbook of Magnetic Materials*, edited by K. H. J. Buschow (Elsevier, Amsterdam, 2001), Vol. 13.
[4] K. Sato, H. Kida, and T. Kamimura, J. Magn. Soc. Jpn. **11**, 113 (1987).
[5] N. Fang, H. Lee, C. Sun, and X. Zhang, Science **308**, 534 (2005).
[6] A. N. Grigorenko, A. K. Geim, H. F. Gleeson, Y. Zhang, A. A. Firsov, I. Y. Khrushchev, and J. Petrovic, Nature (London) **438**, 335 (2005).
[7] C. C. Homes and T. Vogt, Nat. Mater. **12**, 782 (2013).
[8] C. Della Giovampaola and N. Engheta, Nat. Mater. **13**, 1115 (2014).
[9] J. Sun, M. I. Shalaev, N. M. Litchinitser, G. Bartal, and X. Zhang, Nat. Commun. **6**, 7201 (2015).

[10] S. A. R. Horsley, M. Artoni, and G. C. La Rocca, Nat. Photonics **9**, 436 (2015).
[11] M. V. Rybin, D. S. Filonov, K. B. Samusev, P. A. Belov, Y. S. Kivshar, and M. F. Limonov, Nat. Commun. **6**, 10102 (2015).
[12] I. Liberal and N. Engheta, Nat. Photonics **11**, 149 (2017).
[13] N. Mojarad, J. Gobrecht, and Y. Ekinci, Sci. Rep. **5**, 9235 (2015).
[14] E. Ferrari, E. Allaria, J. Buck, G. De Ninno, B. Diviacco, D. Gauthier, L. Giannessi, L. Glaser, Z. Huang, M. Ilchen, G. Lambert, A. A. Lutman, B. Mahieu, G. Penco, C. Spezzani, and J. Viefhaus, Sci. Rep. **5**, 13531 (2015).
[15] H. Yan, C. Wang, A. R. McCarn, and H. Ade, Phys. Rev. Lett. **110**, 177401 (2013).
[16] L. Pasquali, S. Mukherjee, F. Terzi, A. Giglia, N. Mahne, K. Koshmak, V. Esaulov, C. Toccafondi, M. Canepa, and S. Nannarone, Phys. Rev. B **89**, 045401 (2014).
[17] K. Sato, Jpn. J. Appl. Phys. **20**, 2403 (1981).
[18] M. Suzuki, N. Kawamura, M. Mizumaki, A. Urata, H. Maruyama, S. Goto, and T. Ishikawa, Jpn. J. Appl. Phys. **37**, L1488 (1998).
[19] E. E. Koch, D. E. Eastman, and Y. Farge, in *Handbook on Synchrotron Radiation*, edited by E. E. Koch (North-Holland, Amsterdam, 1983), Vol. 1A, pp. 1–63.
[20] S. Krinsky, M. L. Perlman, and R. E. Watson, in *Handbook on Synchrotron Radiation*, edited by E. E. Koch (North-Holland, Amsterdam, 1983), Vol. 1A, pp. 65–171.
[21] M. Terasawa and M. Kihara, in *Applications of Synchrotron Radiation to Materials Analysis*, edited by H. Saisho and Y. Gohshi (Elsevier, Amsterdam, 1996), pp. 1–78.
[22] C. T. Chen, Y. U. Idzerda, H. J. Lin, N. V. Smith, G. Meigs, E. Chaban, G. H. Ho, E. Pellegrin, and F. Sette, Phys. Rev. Lett. **75**, 152 (1995).
[23] J. B. Kortright and S.-K. Kim, Phys. Rev. B **62**, 12216 (2000).
[24] J. Kunes, P. M. Oppeneer, H.-C. Mertins, F. Schäfers, A. Gaupp, W. Gudat, and P. Novak, Phys. Rev. B **64**, 174417 (2001).
[25] H.-C. Mertins, O. Zaharko, A. Gaupp, F. Schäfers, D. Abramsohn, and H. Grimmer, J. Magn. Magn. Mater. **240**, 451 (2002).
[26] H.-C. Mertins, S. Valencia, D. Abramsohn, A. Gaupp, W. Gudat, and P. M. Oppeneer, Phys. Rev. B **69**, 064407 (2004).
[27] S. Valencia, H.-C. Mertins, D. Abramsohn, A. Gaupp, W. Gudat, and P. M. Oppeneer, Phys. B **345**, 189 (2004).
[28] A. Scherz, E. K. U. Gross, H. Appel, C. Sorg, K. Baberschke, H. Wende, and K. Burke, Phys. Rev. Lett. **95**, 253006 (2005).
[29] J. B. Kortright, J. Electron Spectrosc. Relat. Phenom. **189**, 178 (2013).
[30] M. F. Tesch, M. C. Gilbert, H.-C. Mertins, D. E. Bürgler, U. Berges, and C. M. Schneider, Appl. Opt. **52**, 4294 (2013).
[31] J. P. van der Ziel, P. S. Pershan, and L. D. Malmstrom, Phys. Rev. Lett. **15**, 190 (1965).
[32] A. Kirilyuk, A. V. Kimel, and T. Rasing, Rev. Mod. Phys. **82**, 2731 (2010).
[33] S. Yamamoto *et al.*, J. Synchrotron Radiat. **21**, 352 (2014).
[34] I. Matsuda, A. Kuroda, J. Miyawaki, Y. Kosegawa, S. Yamamoto, T. Seike, T. Bizen, Y. Harada, T. Tanaka, and H. Kitamura, Nucl. Instrum. Methods Phys. Res., **767**, 296 (2014).
[35] H. Akai, http://kkr.issp.u-tokyo.ac.jp.
[36] H. Akai, J. Phys: Condens. Matter **1**, 8045 (1989).
[37] Y. Kubota, Sh. Yamamoto, T. Someya, Y. Hirata, K. Takubo, M. Araki, M. Fujisawa, K. Yamamoto, Y. Yokoyama, M. Taguchi, S. Yamamoto, M. Tsunoda, H. Wadati, S. Shin, and I. Matsuda, J. Electron Spectros. Relat. Phenom. **220**, 17 (2017).
[38] Y. Kubota, M. Taguchi, H. Akai, Sh. Yamamoto, T. Someya, Y. Hirata, K. Takubo, M. Araki, M. Fujisawa, K. Yamamoto, Y. Yokoyama, S. Yamamoto, M. Tsunoda, H. Wadati, S. Shin, and I. Matsuda, Phys. Rev. B **96**, 134432 (2017).
[39] L. Henke, E. Gullikson, and J. C. Davis, http://www-cxro.lbl.gov/optical_constants/asf.html.